molecules

MDPI

Article

Electronic Structure of C_{60}/Zinc Phthalocyanine/V_2O_5 Interfaces Studied Using Photoemission Spectroscopy for Organic Photovoltaic Applications

Chang Jin Lim [1], Min Gyu Park [1], Min Su Kim [2], Jeong Hwa Han [2], Soohaeng Cho [1], Mann-Ho Cho [2], Yeonjin Yi [2], Hyunbok Lee [3] and Sang Wan Cho [1,*]

1 Department of Physics, Yonsei University, 1 Yonseidae-gil, Wonju-si, Gangwon-do 26493, Korea; eyepiece89@yonsei.ac.kr (C.J.L.); ham744@naver.com (M.G.P.); shcho@yonsei.ac.kr (S.C.)
2 Institute of Physics and Applied Physics, Yonsei University, 50 Yonsei-ro, Seodaemun-Gu, Seoul 03722, Korea; kimssu98k@yonsei.ac.kr (M.S.K.); jh-han@yonsei.ac.kr (J.H.H.); mh.cho@yonsei.ac.kr (M.-H.C.); yeonjin@yonsei.ac.kr (Y.Y.)
3 Department of Physics, Kangwon National University, 1 Gangwondaehak-gil, Chuncheon-si, Gaongwon-do 24341, Korea; hyunbok@kangwon.ac.kr
* Correspondence: dio8027@yonsei.ac.kr; Tel.: +82-33-760-2232

Received: 13 January 2018; Accepted: 14 February 2018; Published: 18 February 2018

Abstract: The interfacial electronic structures of a bilayer of fullerene (C_{60}) and zinc phthalocyanine (ZnPc) grown on vanadium pentoxide (V_2O_5) thin films deposited using radio frequency sputtering under various conditions were studied using X-ray and ultraviolet photoelectron spectroscopy. The energy difference between the highest occupied molecular orbital (HOMO) level of the ZnPc layer and the lowest unoccupied molecular orbital (LUMO) level of the C_{60} layer was determined and compared with that grown on an indium tin oxide (ITO) substrate. The energy difference of a heterojunction on all V_2O_5 was found to be 1.3~1.4 eV, while that on ITO was 1.1 eV. This difference could be due to the higher binding energy of the HOMO of ZnPc on V_2O_5 than that on ITO regardless of work functions of the substrates. We also determined the complete energy level diagrams of C_{60}/ZnPc on V_2O_5 and ITO.

Keywords: organic photovoltaics; photoemission spectroscopy; energy band diagram; ZnPc; V_2O_5

1. Introduction

Organic photovoltaics (OPVs) have received increasing attention over the past few years due to their potential as a renewable, cheap, and economical source of power [1–6]. However, despite significant recent advances in their cell performance, the current power conversion efficiencies remain too low for commercial viability of such cells. A general problem of organic electronic devices is the poor transport of charge carriers at the interface between electrodes and the organic semiconductor. Consequently, recent efforts have been made to improve charge transport and collection at the electrodes. In particular, the use of transition metal oxides as a transparent electrode has attracted considerable interest [7]. Indium tin oxide (ITO) is widely used as an electrode in OPV fabrication and as a transparent conducting electrode for light-emitting diodes due to its reasonable transparency in the visible region, good conductivity, and ease of patterning. However, the surface chemistry of ITO is difficult to control [8] and ITO has become approximately 10 times more expensive over the past few years due to diminishing indium resources [9]. In fact, the cost of indium is expected to increase because of the increasing demand from producers of solar cells in addition to the demand from the existing flat-panel display industry [10]. Transition metal oxides are believed to prevent unwanted chemical reactions between transparent electrodes and an optically active organic layer [11–13]. Furthermore,

a high work function material such as a metal oxide is desirable to decrease the series resistance in devices [14]. Due to different oxidation states, vanadium can be used to create many compounds with oxygen such as vanadium monoxide (VO), vanadium sesquioxide (V_2O_3), vanadium dioxide (VO_2), vanadium pentoxide (V_2O_5), V_3O_7, V_6O_{13}, and V_4O_9 [15], which exhibit specific properties depending on structure. At a critical temperature, crystallographic transformation shows that vanadium oxide accompanies a reversible semiconductor-to-metal transition that alters its optical and electrical properties [16]. Among the possible compounds of vanadium oxides, the stable V_2O_5 phase possesses a wide optical band gap, good chemical and thermal stability, and excellent thermoelectric properties, which suggest that V_2O_5 is a potential candidate in several applications including electro-chromic displays, gas sensing, and optoelectronic devices [17–20]. Different deposition techniques such as spray pyrolysis, ultrasonic spray pyrolysis, spin coating, thermal evaporation, electron beam evaporation, radio frequency sputtering, dc magnetron sputtering, sol-gel, and chemical vapor deposition have been used to deposit vanadium oxide thin films in order to improve the optical and electrical properties of transparent conductive oxides (TCOs).

In this study, the electronic structures and energy level alignment of a bilayer of C_{60} and ZnPc grown on V_2O_5 thin films deposited using radio frequency sputtering under various conditions were studied. The electronic structure was measured using in-situ ultraviolet photoemission spectroscopy (UPS) and X-ray photoemission spectroscopy (XPS). The separation of the highest occupied molecular orbital (HOMO) of the donor and the lowest unoccupied molecular orbital (LUMO) of the acceptor (E^D_{HOMO}–E^A_{LUMO}) was measured for each bilayer because E^D_{HOMO}–E^A_{LUMO} is a strong factor in determining the magnitude of the measured open circuit voltage (V_{OC}) of an OPV cell based on a donor–acceptor heterojunction [21,22].

2. Results and Discussion

As shown in Table 1, V_2O_5 samples were fabricated under three different growth conditions. The V_2O_5 #1 sample was grown in an Ar atmosphere for 5 min, and the V_2O_5 #2 sample was grown in an Ar atmosphere for 20 min. Alternatively, the V_2O_5 #3 sample was deposited in an Ar:O2 atmosphere (at a ratio of 29:1) for 20 min. The sheet resistances of the samples were not significantly different.

Table 1. The growth conditions of V_2O_5 #1, #2, and #3.

V_2O_5 #1	
Growth time (min)	5
Gas flow (sccm)	Ar = 30
Sheet resistivity (Ω/sq.)	48
V_2O_5 #2	
Growth time (min)	20
Gas flow (sccm)	Ar = 30
Sheet resistivity (Ω/sq.)	46
V_2O_5 #3	
Growth time (min)	20
Gas flow (sccm)	Ar:O2 = 29:1
Sheet resistivity (Ω/sq.)	36

To determine the chemical state of the elements in the obtained samples, XPS analysis was carried out. These results are shown in Figure 1. For vanadium, a complex energy distribution of V 2*p* photoelectrons was obtained. The V 2*p* core level spectrum is dominated by a spin-orbit doublet with peaks at binding energies of about 517.5 and 525.0 eV. Both the binding energy and spin-orbit splitting are in good agreement with values previously reported for V_2O_5 [23]. The line shapes of these spectra were analyzed by a standard least squares fitting scheme using a convolution of Gaussian and Lorentzian peaks. The width of the Lorentzian peaks was assumed to be the same for each component.

We obtain an fwhm for the Lorentzian of about 0.35 eV for V $2p_{3/2}$. The FWHM for the Gaussian resulting from the fitting procedure is 1.20~1.40 eV. As shown in Figure 1a, an additional peak in the V $2p_{3/2}$ core level was also observed at lower binding energy (about 516.4 eV) in all samples; however, the relative intensity of that in V_2O_5 #1 was greater than in the others. The peak position is close to that reported for single crystalline VO_2 [23]. The oxidation states of vanadium V_2O_5 and VO_2 are V^{5+} and V^{4+}, respectively. This means that the V_2O_5 #1 sample did not have enough deposition time to form a perfect composition and had relatively more oxygen vacancies, which account for the higher defect level and greater abundance of trap-assisted conducting oxides than in the others. In Figure 1b, an additional O 1*s* core level was also observed at higher binding energies in all samples. The relative intensity of that of V_2O_5 #1 is also greater than the others in the O 1*s* core level spectra.

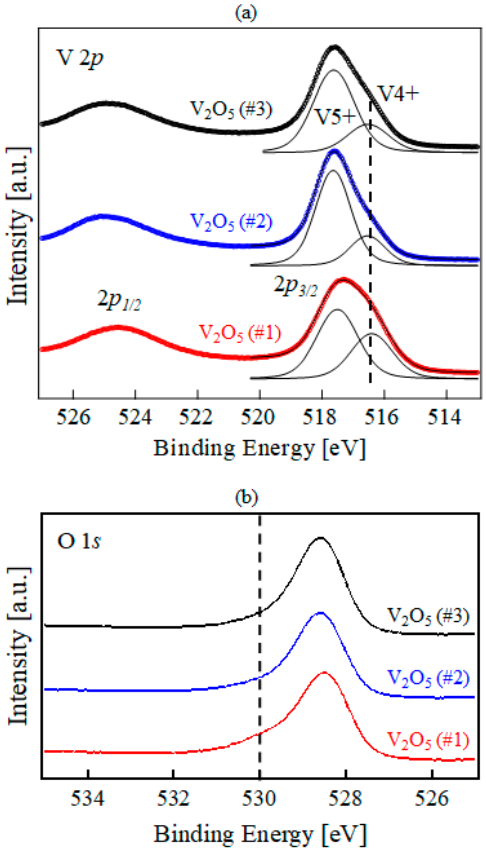

Figure 1. (**a**) V 2*p* and (**b**) O 1*s* core level photoemission spectra of V_2O_5 #1, V_2O_5 #2, and V_2O_5 #3, measured with a monochromatic Al Ka X-ray source.

The electronic structures during the interface formation of C_{60}/ZnPc/V_2O_5 #1, #2, and #3 were investigated using in-situ UPS. Figures 2 and 3 show UPS spectra obtained for the deposition of C_{60}/ZnPc on various V_2O_5 thin films. The spectra shown in Figure 2a–c were collected in the secondary electron cut-off region for the V_2O_5 #1, V_2O_5 #2, and V_2O_5 #3 layers, respectively. The supplementary material (Figure S1) illustrates the procedure used for the determination of energy-level alignment at the interface. The secondary cut-off position moved noticeably toward a higher binding energy as soon as the ZnPc deposition began on each substrate. The shift of the secondary cut-off position is attributed to the formation of an interface dipole and band bending [24,25]. However, the secondary cut-off position moved toward lower binding energies as soon as C_{60} deposition began on each ZnPc layer. In these spectra, the total shift of the cut-off position of ZnPc toward higher binding energies was 0.45, 0.50, and 0.25 eV, while that of C_{60} on the ZnPc layer was 0.35, 0.20, and 0.15 eV toward lower binding energies for V_2O_5 #1, V_2O_5 #2, and V_2O_5 #3, respectively.

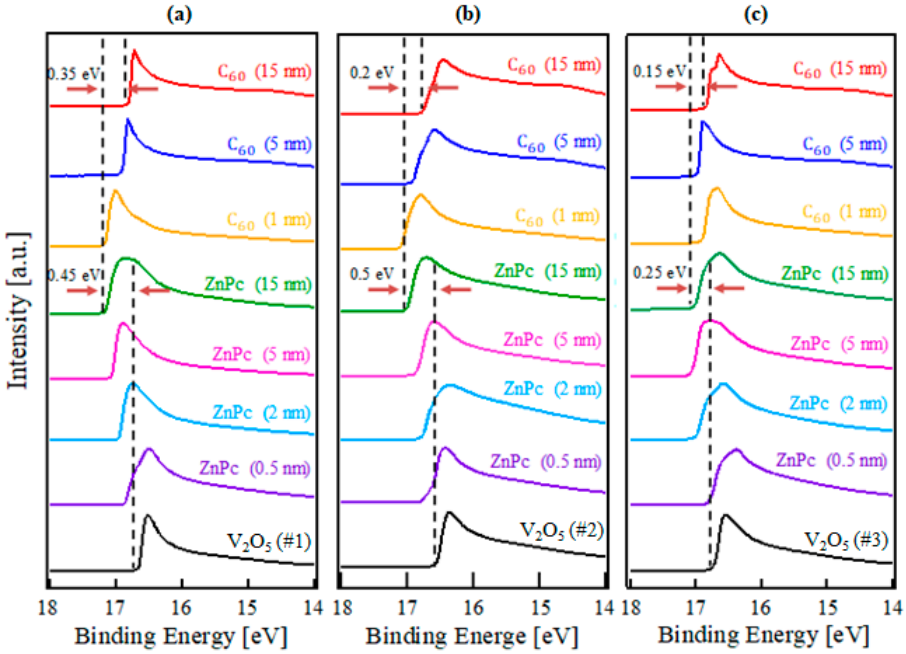

Figure 2. The UPS spectra in the secondary cut-off region collected during the step-by-step layer deposition of C_{60}/ZnPc on (**a**) V_2O_5 #1, (**b**) V_2O_5 #2, and (**c**) V_2O_5 #3 surfaces.

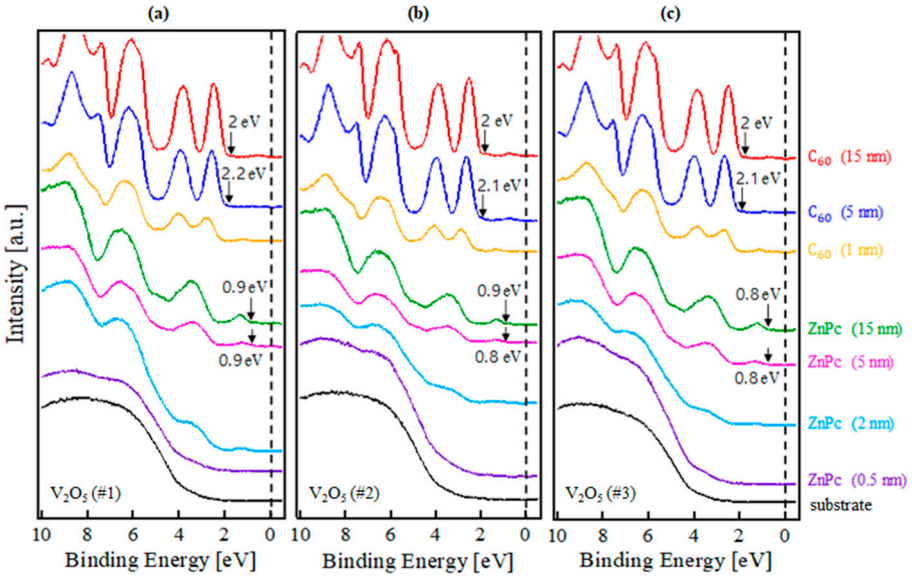

Figure 3. The UPS spectra collected near the Fermi level as a function of the C_{60}/ZnPc deposition thickness on (**a**) V_2O_5 #1, (**b**) V_2O_5 #2, and (**c**) V_2O_5 #3 surfaces.

Figure 3a–c show the evolution of HOMO onset during the growth of the C_{60}/ZnPc layer on V_2O_5 #1, V_2O_5 #2, and V_2O_5 #3, respectively. As shown in Figure 3a, there was no shift in HOMO onset of ZnPc for the ZnPc/V_2O_5 #1 interface and the HOMO onset was measured at 0.9 eV below the Fermi level. It is clear that the HOMO of C_{60} gradually shifted toward lower binding energies, and total shift reached 0.2 eV after the shifts were saturated. This result confirms that band bending occurred at the C_{60}/ZnPc interface. The saturated HOMO onset of the C_{60} layer was 2.0 eV below the Fermi level. In Figure 3b, the HOMO onset of ZnPc gradually shifted toward higher binding energies from 0.8 to 0.9 eV, confirming band bending at the ZnPc/V_2O_5 #2 interface. It was also observed that the HOMO of C_{60} gradually shifted toward lower binding energies, and the total shift reached 0.1 eV.

The saturated HOMO onset of the C_{60} layer was 2.0 eV below the Fermi level. In Figure 3c, the HOMO onset of ZnPc on V_2O_5 #3 did not shift, and the HOMO onset was measured at 0.8 eV below the Fermi level. The HOMO of C_{60} shifted toward lower binding energies from 2.1 to 2.0 eV.

An energy level diagram was constructed by combining the changes of the spectra shown in Figures 2 and 3. We estimate that the overall measurement errors in orbital offsets and interface dipoles are of the order of ±0.05 eV. We determined the energy positions according to the systematic procedure as described in detail in [7]. Additionally, the energy level diagram of C_{60}/ZnPc/ITO based on our data (not shown here) is displayed. As shown in Figure 4, the energy gaps between the HOMO and LUMO of ZnPc and C_{60} were about 1.9 and 2.6 eV, respectively, as previously reported [26,27]. The measured work functions of V_2O_5 #1, V_2O_5 #2, and V_2O_5 #3 were estimated to be about 4.5, 4.7, and 4.5 eV, respectively. The energy level difference between the HOMO of the donor (ZnPc) and the LUMO of the acceptor (C_{60}), E^D_{HOMO}–E^A_{LUMO} is an important factor in determining the magnitude of V_{OC} of OPVs based on a donor–acceptor heterojunction. However, a correction term between the real V_{OC} and the E^D_{HOMO}–E^A_{LUMO} value may be required to account for voltage losses in the device due to large diode quality factors, high reverse saturation currents, low-field-dependent mobilities of charge carriers, and voltage losses at the collection electrodes.

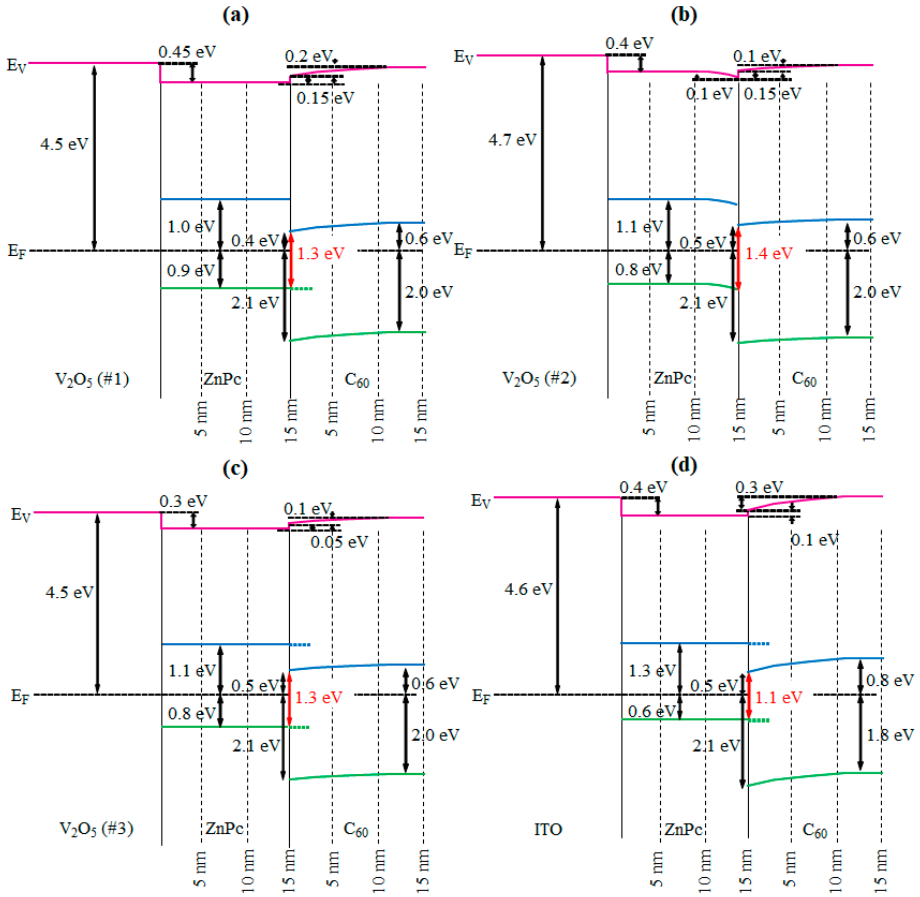

Figure 4. Energy level diagrams of C_{60}/ZnPc on (**a**) V_2O_5 #1, (**b**) V_2O_5 #2, (**c**) V_2O_5 #3, and (**d**) ITO surfaces.

The C_{60}/ZnPc heterojunction on V_2O_5 #2 showed the largest E^D_{HOMO}–E^A_{LUMO} value (1.4 eV). The measured E^D_{HOMO}–E^A_{LUMO} values on V_2O_5 #1 and V_2O_5 #3 were the same (1.3 eV). There are several factors that can affect the magnitude of E^D_{HOMO}–E^A_{LUMO} at the donor–acceptor interface, including the ionization potential of a donor, the electron affinity of an acceptor, the formation of interface dipoles, and charge redistribution across the interfaces. In this case, the band bending of ZnPc

was observed only at the ZnPc/V_2O_5 #2 interface, and the band bending moved the HOMO of the donor (ZnPc) toward higher binding energies and increased the E^D_{HOMO}–E^A_{LUMO} value. In general, this is due to different degrees of charge transfer from the substrate to the ZnPc layer, and the work function difference of substrates is the origin of the different degrees of charge transfer. However, the value of band bending (0.1 eV) was almost negligible considering the measurement error. Therefore, this 0.1 eV difference of the E^D_{HOMO}–E^A_{LUMO} value was not predicted to lead to enhanced values of V_{OC} for OPVs. On the other hand, the measured E^D_{HOMO}–E^A_{LUMO} values on ITO was 1.1 eV, which is smaller than those on V_2O_3 samples. This means that the OPV using V_2O_3 as an anode should have a larger V_{OC} than that using ITO. This is because the HOMO onset of ZnPc on ITO was 0.2~0.3 eV lower than that on the V_2O_5 regardless of work functions of the substrates. To understand the underlying cause, further studies should be conducted comparing the charge neutrality level of ZnPc with the density of states of V_2O_5 and ITO. Therefore, not only the work functions of new TCOs but also the charge neutrality level of donors should be considered for controlling the V_{OC} for high-efficiency OPVs.

3. Methods

V_2O_5 films on ITO substrate were prepared by radio frequency magnetron sputtering of V_2O_5 targets at room temperature. Before deposition the ITO substrates were sequentially cleaned ultrasonically in acetone, alcohol, and de-ionized water before finally being dried in nitrogen gas. The distance between the target and substrate was approximately 100 mm. The radio frequency magnetron working power was 200 W, and deposition times were 5 and 20 min. The base pressure was 5.7×10^{-7} Torr and the working pressure was 2.5 m Torr. As shown in Table 1, three V_2O_5 films at different deposition times and flowing gas compositions were prepared.

The chemical states for the V_2O_5 films grown on ITO were examined by XPS. XPS core level spectra of V 2*p* and O 1*s* were obtained using a monochromatic Al Ka X-ray source. In situ UPS measurements were carried out using a PHOIBOS 150 energy analyzer (SPECS GmbH, Berlin, Germany) and an ultraviolet (He I, 21.22 eV) light source. The base pressure of the analysis chamber was 5×10^{-10} Torr. ZnPc and C_{60} were thermally evaporated on V_2O_5 and ITO substrates at a rate of 0.01 nm/s. The total thickness and deposition rate were monitored by a quartz crystal microbalance. The secondary electron cut-off (SEC) positions were measured in normal emission geometry with a sample bias of −5 V.

4. Conclusions

The interfacial electronic structures of a bilayer of C_{60} and ZnPc grown on V_2O_5 thin films deposited using radio frequency sputtering under various conditions were studied using X-ray and ultraviolet photoelectron spectroscopy. The energy difference between the HOMO level of the ZnPc layer and the LUMO level of the C_{60} layer was determined and compared with that grown on ITO substrate. The energy difference of a heterojunction on all V_2O_5 was found to be 1.3~1.4 eV, while that on ITO was 1.1 eV. This difference could be due to the HOMO of ZnPc on V_2O_5 having a higher binding energy than that on ITO regardless of work functions of the substrates. We also determined the complete energy level diagrams of C_{60}/ZnPc on V_2O_5 and ITO.

Supplementary Materials: The Supplementary Materials are available online.

Acknowledgments: This research was supported by the Basic Science Research Programs through the National Research Foundation of Korea (Grant No. NRF-2017R1D1A3B03034867) and Yonsei University Wonju Campus Future-leading Research Initiative (Grant No. 2017-52-0071)

Author Contributions: C.J.L. and S.W.C. designed the experiment. C.J.L., M.G.P., M.S.K., and J.H.H. performed the experiments and analyzed the data. C.J.L. and S.W.C. wrote the main manuscript text. S.C. Y.Y., M.-H.C., and H.L. participated in discussion through the work.

Conflicts of Interest: The authors declare no conflict of interest.

References

1. Peng, Y.; Yaacobi-Gross, N.; Perumal, A.K.; Faber, H.A.; Vourlias, G.; Patsalas, P.A.; Bradley, D.D.C.; He, Z.Q.; Anthopoulos, T.D. Efficient organic solar cells using copper(I) iodide (CuI) hole transport layers. *Appl. Phys. Lett.* **2015**, *106*. [CrossRef]
2. Falke, S.M.; Rozzi, C.A.; Brida, D.; Maiuri, M.; Amato, M.; Sommer, E.; De Sio, A.; Rubio, A.; Cerullo, G.; Molinari, E.; et al. Coherent ultrafast charge transfer in an organic photovoltaic blend. *Science* **2014**, *344*, 1001–1005. [CrossRef] [PubMed]
3. Sullivan, P.; Duraud, A.; Hancox, I.; Beaumont, N.; Mirri, G.; Tucker, J.H.R.; Hatton, R.A.; Shipman, M.; Jones, T.S. Halogenated boron subphthalocyanines as light harvesting electron acceptors in organic photovoltaics. *Adv. Energy Mater.* **2011**, *1*, 352–355. [CrossRef]
4. Silvestri, F.; Marrocchi, A.; Seri, M.; Kim, C.; Marks, T.J.; Facchetti, A.; Taticchi, A. Solution-processable low-molecular weight extended arylacetylenes: Versatile p-Type semiconductors for field-effect transistors and bulk heterojunction solar cells. *J. Am. Chem. Soc.* **2010**, *132*, 6108–6123. [CrossRef] [PubMed]
5. Brabec, C.J. Organic photovoltaics: Technology and market. *Sol. Energy Mater. Sol. C* **2004**, *83*, 273–292. [CrossRef]
6. Garcias-Morales, C.; Romero-Borja, D.; Maldonado, J.-L.; Roa, A.; Rodríguez, M.; García-Merinos, J.; Ariza-Castolo, A. Small molecules derived from Thieno[3,4-c]pyrrole-4,6-dione (TPD) and their use in solution processed organic solar cells. *Molecules* **2017**, *22*. [CrossRef] [PubMed]
7. Lee, H.; Cho, S.W.; Yi, Y. Interfacial electronic structure for high performance organic devices. *Curr. Appl. Phys.* **2016**, *16*, 1533–1549. [CrossRef]
8. Kim, J.S.; Friend, R.H.; Grizzi, I.; Burroughes, J.H. Spin-cast thin semiconducting polymer interlayer for improving device efficiency of polymer light-emitting diodes. *Appl. Phys. Lett.* **2005**, *87*. [CrossRef]
9. Bhosle, V.; Prater, J.T.; Yang, F.; Burk, D.; Forrest, S.R.; Narayan, J. Gallium-doped zinc oxide films as transparent electrodes for organic solar cell applications. *J. Appl. Phys.* **2007**, *102*. [CrossRef]
10. Murdoch, G.B.; Hinds, S.; Sargent, E.H.; Tsang, S.W.; Mordoukhovski, L.; Lu, Z.H. Aluminum doped zinc oxide for organic photovoltaics. *Appl. Phys. Lett.* **2009**, *94*. [CrossRef]
11. Shrotriya, V.; Li, G.; Yao, Y.; Chu, C.W.; Yang, Y. Transition metal oxides as the buffer layer for polymer photovoltaic cells. *Appl. Phys. Lett.* **2006**, *88*. [CrossRef]
12. Zou, J.Y.; Li, C.Z.; Chang, C.Y.; Yip, H.L.; Jen, A.K.Y. Interfacial engineering of ultrathin metal film transparent electrode for flexible organic photovoltaic cells. *Adv. Mater.* **2014**, *26*, 3618–3623. [CrossRef] [PubMed]
13. Heo, N.; Kim, Y.; Jung, Y.; Cheon, S.; Cho, S.; Cho, S.W.; Park, S.; Yi, Y.; Smith, K.E. Interfacial electronic structure of C-60/ZnPc/AZO on photoemission spectroscopy for organic photovoltaic applications. *Chem. Phys.* **2016**, *478*, 145–149. [CrossRef]
14. Cattin, L.; Dahou, F.; Lare, Y.; Morsli, M.; Tricot, R.; Houari, S.; Mokrani, A.; Jondo, K.; Khelil, A.; Napo, K.; et al. MoO_3 surface passivation of the transparent anode in organic solar cells using ultrathin films. *J. Appl. Phys.* **2009**, *105*. [CrossRef]
15. Beke, S. A review of the growth of V_2O_5 films from 1885 to 2010. *Thin Solid Films* **2011**, *519*, 1761–1771. [CrossRef]
16. Morin, F.J. Oxides which show a metal-to-insulator transition at the neel temperature. *Phys. Rev. Lett.* **1959**, *3*, 34–36. [CrossRef]
17. Iida, Y.; Kaneko, Y.; Kanno, Y. Fabrication of pulsed-laser deposited V_2O_5 thin films for electrochromic devices. *J. Mater. Process. Technol.* **2008**, *197*, 261–267. [CrossRef]
18. Luo, Z.; Wu, Z.; Xu, X.; Du, M.; Wang, T.; Jiang, Y. Impact of substrate temperature on the microstructure, electrical and optical properties of sputtered nanoparticle V_2O_5 thin films. *Vacuum* **2010**, *85*, 145–150. [CrossRef]
19. Mousavi, M.; Kompany, A.; Shahtahmasebi, N.; Bagheri-Mohagheghi, M.M. Effect of S-doping on structural, optical and electrochemical properties of vanadium oxide thin films prepared by spray pyrolysis. *Phys. Scr.* **2013**, *88*. [CrossRef]
20. Mousavi, M.; Kompany, A.; Shahtahmasebi, N.; Bagheri-Mohagheghi, M.M. Study of structural, electrical and optical properties of vanadium oxide condensed films deposited by spray pyrolysis technique. *Adv. Manuf.* **2013**, *1*, 320–328. [CrossRef]

21. Piper, L.F.J.; Cho, S.W.; Zhang, Y.; DeMasi, A.; Smith, K.E.; Matsuura, A.Y.; McGuinness, C. Soft X-ray spectroscopy study of the element and orbital contributions to the electronic structure of copper hexadecafluoro-phthalocyanine. *Phys. Rev. B* **2010**, *81*, 1–12. [CrossRef]
22. Chauhan, V.; Hatton, R.; Sullivan, P.; Jones, T.; Cho, S.W.; Piper, L.; deMasi, A.; Smith, K. Elucidating the factors that determine the open circuit voltage in discrete heterojunction organic photovoltaic cells. *J. Mater. Chem.* **2010**, *20*, 1173–1178. [CrossRef]
23. Demeter, M.; Neumann, M.; Reichelt, W. Mixed-valence vanadium oxides studied by XPS. *Surf. Sci.* **2000**, *454–456*, 41–44. [CrossRef]
24. Lee, S.T.; Hou, X.Y.; Mason, M.G.; Tang, C.W. Energy level alignment at Alq/metal interfaces. *Appl. Phys. Lett.* **1998**, *72*, 1593–1595. [CrossRef]
25. Ishii, H.; Sugiyama, K.; Ito, E.; Seki, K. Energy level alignment and interfacial electronic structures at organic metal and organic organic interfaces. *Adv. Mater.* **1999**, *11*, 605–625. [CrossRef]
26. Gao, W.Y.; Kahn, A. Electronic structure and current injection in zinc phthalocyanine doped with tetrafluorotetracyanoquinodimethane: Interface versus bulk effects. *Org. Electron.* **2002**, *3*, 53–63. [CrossRef]
27. Mitsumoto, R.; Seki, K.; Araki, T.; Ito, E.; Ouchi, Y.; Achiba, Y.; Kikuchi, K.; Yajima, S.; Kawasaki, S.; Okino, F.; et al. Soft X-ray absorption, UV photoemission, and VUV absorption spectroscopic studies of fluorinated fullerenes. *J. Electron. Spectrosc. Relat. Phenom.* **1996**, *78*, 453–456. [CrossRef]

Sample Availability: Samples of the compounds are not available from the authors.